AMERICAN METEOROLOGICAL SOCIETY

Journal of Physical Oceanography

EARLY ONLINE RELEASE

The DOI for this manuscript is doi: 10.1175/JPO-D-11-0200.1

The final published version of this manuscript will replace the preliminary version at the above DOI once it is available.

If you would like to cite this EOR in a separate work, please use the following full citation:

Huisman, S., H. Dijkstra, A. von der Heydt, and W. de Ruijter, 2012: Does net E-P set a preference for North Atlantic sinking? J. Phys. Oceanogr. doi:10.1175/JPO-D-11-0200.1, in press.

Does net $E - P$ set a preference for North Atlantic sinking?

Selma E. Huisman, Henk A. Dijkstra[1], A. S. von der Heydt, and W. P. M. de Ruijter

Institute for Marine and Atmospheric research Utrecht (IMAU)
Department of Physics and Astronomy, Utrecht University
Princetonplein 5, 3584 Utrecht, the Netherlands

Revised for J. Phys. Oceanography

Version of April 16, 2012

[1]Correspondence: Email: H.A.Dijkstra@uu.nl

Abstract

The present-day global Meridional Overturning Circulation (MOC) with formation of North Atlantic Deep Water (NADW) and the absence of a deep water formation in the North Pacific, is often considered to be caused by the fact that the North Pacific basin is a net precipitative, while the North Atlantic is a net evaporative basin. In this paper, we study the effect of asymmetries in continent geometry and freshwater fluxes on the MOC both in an idealized two-dimensional model and in a global ocean model. We approach the problem from a multiple equilibria perspective where asymmetries in external factors constrain the existence of steady MOC patterns. Both this multiple equilibria perspective and the fact that we use a realistic global geometry add new aspects to the problem. In the global model, it is shown that the Atlantic forced by net precipitation can have a meridional overturning circulation with northern sinking and a sea surface salinity that resembles the present-day salinity field. The model results are suggestive of the importance of factors other than the freshwater flux asymmetries, in particular continental asymmetries, in producing the meridional overturning asymmetry.

1 Introduction

A key feature of the global ocean circulation is its Atlantic–Pacific asymmetry, with only deep water formation in the North Atlantic and not in the Pacific. About half of the meridional heat transport in the North Atlantic at 26°N (about 1.5 PW) is attributed to deep water formation [Talley, 2003; Ferrari and Ferreira, 2011]. The difference in sea surface salinity (SSS) between the basins can explain this asymmetry; Pacific upper layer water is too fresh to sink to great depths, even when it is cooled to the freezing point [Warren, 1983]. This salinity difference is thought to be caused by net precipitation (P) in the Pacific and net evaporation (E) in the Atlantic, together with moisture transport through the atmosphere out of the Atlantic and into the Pacific over the Central American isthmus (the "atmospheric bridge" [Zaucker et al., 1994]).

Emile-Geay et al. [2003] analyzed the freshwater budgets for the northern North Atlantic (nNA) and northern North Pacific (nNP), between latitudes 43°N and 60°N, and found that the precipitation over the nNP is about 0.2 Sv larger than over the nNA. They attributed this to a limited ocean cross-gyre exchange in the nNP and to moisture transport associated with the strength of the Asian monsoon. When considered per unit area, however, the net evaporation is a factor 1.6 times larger in the nNA ($E = 2.75 \times 10^{-5}$ kg m^{-2} s^{-1}) than in the nNP ($E = 1.70 \times 10^{-5}$ kg m^{-2} s^{-1}) but the precipitation per unit area is very similar in both basins ($P = 3.47 \times 10^{-5}$ kg m^{-2} s^{-1} in the nNP versus $P = 3.28 \times 10^{-5}$ kg m^{-2} s^{-1} in the nNA; note that 10^{-5} kg m^{-2} s^{-1} $\approx$ 0.85 mm/day). The higher evaporation is directly related to the higher surface temperature in the Atlantic Ocean, which in turn is caused by the presence of deep water formation in the Atlantic and the absence of it in the Pacific. One can argue whether the explanation for the Atlantic–

Pacific asymmetry based on the hydrological cycle [Warren, 1983] contains a circular argument [Czaja, 2009] or not, but at least one should explain how external asymmetries (e.g., in continental geometry and the wind stress field), possibly amplified by the salt-advection feedback, lead to the observed asymmetry of the global MOC.

In Czaja [2009] the asymmetries in the wind stress field, in particular the positioning of the gyre boundary with respect the location of the $E = P$ curve, are proposed as an important asymmetry. de Boer et al. [2008] investigate the sensitivity of the dominance of the nNA sinking in an idealized two-basin ocean model coupled to an atmospheric EBM. They find that a strong hydrological cycle (and also weak Southern Ocean winds) will increase this dominance and attribute an important role to geographical factors. Ferreira and Marshall [2010] study flows in a coupled ocean-atmosphere-ice aqua-planet model. In the configuration with a small and a large basin (DDrake) they find that the salinity contrast between the basins (the smaller one being saltier) results from a deficit in precipitation over the small basin.

There is another issue which may be very relevant to the Atlantic-Pacific asymmetry: the existence of multiple equilibria. In an idealized ocean-only model of two (similar-size) basins which are connected by a channel at high southern latitudes, four different equilibrium solutions of the ocean circulation are found under an equatorially symmetric freshwater flux [Marotzke and Willebrand, 1991; Huisman et al., 2009]. The four states are the Conveyor, Inverse Conveyor, Southern Sinking and Northern Sinking, where the Conveyor state is associated with the present-day Atlantic–Pacific asymmetric circulation. Two of these states, the Northern Sinking and Inverse Conveyor, have deep convection in the Pacific.

When asymmetries in Atlantic and Pacific geometry and equatorial asym-

metries in freshwater flux [Zaucker et al., 1994] and those in the atmospheric circulation [Czaja, 2009] are taken into account, it is expected that some of these four states can no longer be maintained as steady states. For example, the presence of open gateways (with relevance to paleocean circulation) has been shown to lead to 'preference' of specific solutions over others [von der Heydt and Dijkstra, 2008]. The preference here indicates that in the relevant parameter volume, some states remain to exist as steady states whereas others cease to exist. Hughes and Weaver [1994] computed only a limited number of steady states but they found that the overall asymmetry of the geometry causes a preference for states with Atlantic deep water formation (see also Weaver et al. [1999]).

The studies on the relevance of multiple equilibria in the Pacific-Atlantic asymmetry problem have so far only been carried out in idealized two-basin configurations. With the results in this paper, we contribute in two ways to the problem of the asymmetry of the global MOC. First, we define the concept of preference of steady states in more detail and second, we consider the relevance of multiple equilibria in a fairly realistic global ocean geometry. In section 2, we use a two-dimensional model to study the effect of equatorially asymmetric freshwater fluxes and continental boundaries on the preference of MOC patterns, and propose to define preference in terms of existence intervals of a steady solution in parameter space. This concept of preference is particularly useful to determine how asymmetries limit regimes of multiple equilibria. Next, we use a global low-resolution ocean model coupled to an energy balance atmosphere model [Dijkstra and Weijer, 2005] to address the Atlantic–Pacific asymmetry problem. We specifically focus on possible global ocean circulation solutions for two different surface freshwater fluxes, where one of them is expected to strongly have a preference for North Pacific sinking

and the other for North Atlantic sinking.

2 MOC preference in a 2D ocean model

To explain the concept of 'preference' due to to asymmetries in freshwater forcing and continental asymmetry in the context of multiple equilibria of the MOC, we study in this section the steady states of a two-dimensional (2D, meridional-depth) ocean model.

2.1 Model formulation

The fully implicit 2D model used in this study is adapted from the model in Weijer and Dijkstra [2001]. In absence of wind-stress forcing and under zero rotation, the solutions are strictly two-dimensional. The model domain is bounded by the latitudes $[75°S, 75°N]$ and has a constant depth of $4\,km$. To allow for a change in continental geometry, we choose a basin geometry as in Fig. 1a with two regions $[75°S, \theta_S]$ and $[\theta_N, 75°N]$ where the ocean is only two grid-points (500 m) deep.

The meridional and vertical velocity components are indicated by v and w, the temperature, salinity and pressure by T, S and p, respectively. Mixing of momentum and of heat and salt is represented by eddy diffusivities, with horizontal and vertical friction coefficients A_H and A_V for momentum and horizontal and vertical diffusivities K_H and K_V for heat and salt. The linear equation of state has expansion coefficients α_T and α_S, with reference temperature T_0, salinity S_0 and density ρ_0. The governing model equations are the two-dimensional hydrostatic Navier-Stokes equations on a spherical

Earth, given by

$$\frac{Dv}{dt} = -\frac{1}{\rho_0 r_0}\frac{\partial p}{\partial \theta} + A_V\frac{\partial^2 v}{\partial z^2} + A_H\left(\frac{1}{r_0^2}\frac{\partial^2 v}{\partial \theta^2} - \frac{v}{r_0^2\cos^2\theta}\right) \tag{1a}$$

$$\frac{\partial p}{\partial z} = -\rho g \tag{1b}$$

$$0 = \frac{\partial w}{\partial z} + \frac{1}{r_0}\frac{\partial v}{\partial \theta} - \frac{v\tan\theta}{r_0} \tag{1c}$$

$$\frac{DT}{dt} = \frac{K_H}{r_0^2\cos\theta}\frac{\partial}{\partial\theta}\Big(\frac{\partial T}{\partial\theta}\cos\theta\Big) + K_V\frac{\partial^2 T}{\partial z^2} \tag{1d}$$

$$\frac{DS}{dt} = \frac{K_H}{r_0^2\cos\theta}\frac{\partial}{\partial\theta}\Big(\frac{\partial S}{\partial\theta}\cos\theta\Big) + K_V\frac{\partial^2 S}{\partial z^2} \tag{1e}$$

$$\rho = \rho_0(1-\alpha_T(T-T_0)+\alpha_S(S-S_0)) \tag{1f}$$

where D/dt indicates the material derivative. Standard values for the dimensional parameters in these equations are listed in Table 1.

On the ocean surface mixed boundary conditions are imposed, i.e. the surface temperature is restored to a profile $T_S(\theta)$ and a freshwater flux F_S is prescribed as a virtual salinity flux. The reference temperature $T_S(\theta)$ has a cosine profile with an amplitude of $\Delta T = 20°C$,

$$T_S(\theta) = T_0 + \frac{\Delta T}{2}\cos\big(\pi\frac{\theta}{\vartheta_0^T}\big) \tag{2}$$

where $\vartheta_0^T = 90°N$. The freshwater flux F_S (E - P) as a function of latitude θ is given by (see Fig. 1b):

$$F_S = \mathcal{A}\,F_0\left[1.2\frac{\cos(\pi\frac{\theta}{\vartheta_0})}{\cos(0.2\,\theta)} - 3\exp\big(\frac{\theta}{0.15\,\vartheta_0}\big)^2 + 0.25\big|\tfrac{\theta}{\vartheta_0}\big| + F_1\tfrac{\theta}{\vartheta_0}\right] + Q \tag{3}$$

where $\mathcal{A} = 10$ mm day^{-1}. Furthermore, F_0 is the dimensionless amplitude of the freshwater flux forcing, F_1 controls the equatorial asymmetry of F_S, $\vartheta_0 = 60°N$ is the location of the midlatitude minimum of F_S and Q is the compensating constant flux to ensure salt conservation. No-slip and no-flux conditions are imposed on the lateral boundaries and bottom boundary.

The model is discretized as described in Weijer and Dijkstra [2001] with a meridional resolution of 3.75° and 16 equidistant vertical layers of thickness $250\,m$. To calculate exact (up to discretization error) steady-state solutions directly as a function of one the parameters of the system (without any time-stepping), we use pseudo-arclength continuation as described in Weijer and Dijkstra [2001]. With this technique, also unstable solutions can be determined (which cannot be reached with a time-marching technique) so that a full bifurcation diagram[2] can be computed [Dijkstra, 2005]. In the results below, we choose the strength of the freshwater flux F_0 as the main control parameter in the bifurcation diagram and fix the southern boundary position $\theta_S = 60°\text{S}$. The equatorial asymmetry of the freshwater forcing is controlled by the parameter F_1 and the continental asymmetry is controlled by the northward extent θ_N.

2.2 Symmetric hemispheric geometry

In the reference case, with $\theta_N = -\theta_S$ and $F_1 = 0$, the basin is of equal size on the northern and southern hemisphere and the freshwater flux is equatorially symmetric. The different steady states found are shown in the bifurcation diagram of Fig. 2a as the drawn curve. On the vertical axis, the sum of the maximum (Ψ_+) and minimum (Ψ_-) value of the meridional overturning streamfunction is plotted. When $\Psi_+ + \Psi_- = 0$ the circulation is equatorially symmetric and two solutions, one with sinking at the poles (indicated below by TH) and one with sinking at the equator (the SA solution) with this property are found. When $\Psi_+ + \Psi_-$ is positive (negative), the northern sinking cell is stronger (weaker) than the southern cell and the solutions are

[2] In a bifurcation diagram, a scalar property of the solution of a model is plotted against a control parameter.

indicated by NPP (SPP), respectively.

In the pure thermal case ($F_0 = 0$) a TH state is found (Fig. 2b), with sinking at the poles and upwelling at the equator. The two-cell TH overturning circulation undergoes spontaneous symmetry breaking (at the pitchfork bifurcation point P_1) due to the salt-advection feedback [Dijkstra and Molemaker, 1997]. The other pitchfork bifurcation (P_2) is associated with a symmetry breaking instability of the SA state. The stability of the different solutions is not indicated here, but can be found for example in Weijer and Dijkstra [2001]. For a certain interval of F_0, solutions coexist and there is a multiple equilibrium regime. For example, for $F_0 = 0.2$ there are three solutions: an NPP (Fig. 2c) solution, an SPP solution and the (unstable) symmetric circulation (the branch connecting P_1 and P_2). The bifurcation diagram for this 2D symmetric reference case is qualitatively similar to that of the 3D model in Weijer and Dijkstra [2001].

When a linear profile is added to the reference surface freshwater flux ($F_1 \neq 0$), the pitchfork bifurcations disappear and isolated branches (Fig. 2, dashed and dotted lines) appear. For example, when $F_1 > 0$, the South Atlantic receives more freshwater than in the reference case (see the dashed curve in Fig. 1b), deep sinking is inhibited in the southern part of the basin and hence the existence interval in F_0 of the SPP solution decreases. The same occurs for the NPP solution when $F_1 < 0$. Therefore, an asymmetric forcing induces a preference for certain solutions (here NPP or SPP) which can be quantified by means of the length of the existence intervals of the stable solutions in the control parameter (here F_0).

The existence intervals of the stable NPP solution for different F_1 are indicated by the stars in the bifurcation diagram (Fig. 2). If for the symmetric case, the existence interval is indicated by $I_0[NPP]$ and for the asymmetric

cases by $I_{F_1}[NPP]$, then the preference of the NPP solution is defined as

$$P_{F_1}[NPP] = \frac{I_{F_1}[NPP]}{I_0[NPP]} \tag{4}$$

When the northern latitudes receive more precipitation (negative F_1) the NPP existence interval is smaller than $I_0[NPP]$ and $P_{F_1}[NPP] < 1$. When the northern latitudes become more evaporative (positive F_1), the existence interval of the NPP solution ($I_{F_1}[NPP]$) becomes larger than $I_0[NPP]$ and hence $P_{F_1}[NPP] > 1$.

Using this concept of preference let us consider that of the NPP solution with asymmetry parameter $F_1 < 0$ and control parameter F_0. For this case, it is found that $P_{F_1}[NPP]$ is a near-linear function of $F_1 < 0$ with slope $s = 5.7$. The critical value for F_{1c} for which the NPP solution disappears is $F_{1c} = -0.19$ (it is just present for $F_1 = -0.15$ in Fig. 2a). This indicates that for $F_1 < F_{1c}$, there is no value of F_0 anymore for which the NPP solution exists. Similarly, we find that $P_{F_1}[SPP]$ is linear for $F_1 > 0$ with the same slope and a critical value $F_{1c} = 0.19$.

To translate this back in a dimensional value of a north-south freshwater flux asymmetry, we note that the difference is the freshwater flux between the asymmetric ($F_1 \neq 0$) and symmetric ($F_1 = 0$) cases is given by

$$F_S^d(\theta) = \mathcal{A} F_0 F_1 \frac{\theta}{\vartheta_0}, \tag{5}$$

When we choose a particular latitude θ_* and consider the north-south difference in the freshwater flux, then we find

$$F_S^d(\theta_*) - F_S^d(-\theta_*) = 2\mathcal{A} F_0 F_1 \frac{\theta_*}{\vartheta_0} \tag{6}$$

Using the reference value of $F_0 = 0.2$ and $\theta_* = 60^\circ$, the freshwater asymmetry due to F_1 is proportional to $2 \cdot 10 \cdot 0.2 \cdot F_1$ mm day^{-1} and so the critical value (for $F_{1c} = -0.19$) corresponds to only 0.76 mm day^{-1}.

2.3 Asymmetric geometry

To test the influence of the continental geometry on the preference of steady solutions in this model, θ_N is shifted both northwards and southwards, while keeping $\theta_S = 60°$S fixed and the freshwater flux symmetric ($F_1 = 0$). In the bifurcation diagrams plotted in Fig. 3a it can be seen how the asymmetry in basin geometry affects the existence intervals in F_0 of the different steady states. For example, the NPP solution exists for a larger range in F_0 when the northern hemispheric basin extents more northward (Fig. 3a, dashed lines). Simultaneously, extending the basin more northward leads to smaller existence intervals for the SPP solution than for the reference case.

The reference existence interval of the NPP solution ($I_0[NPP]$, for $\theta_S = \theta_N = 60°$N) is indicated by the stars on the drawn black line (Fig. 3a). The existence intervals for different basin geometries, $I_{\Delta\theta_N}[NPP]$ are also indicated in Fig. 3a through the stars on the drawn grey curves. It is found that the preference $P_{\Delta\theta_N}[NPP]$ is again a linear function of $\Delta\theta_N$ with a slope $s = 0.044$ (per degree latitude). The critical value for $\Delta\theta_N$ for which the NPP solution disappears is $\Delta\theta_{Nc} = -22°$ (or almost 6 grid-points southwards with respect to the reference case). This appears like a strong geometrical asymmetry compared to the 0.76 mm day^{-1} asymmetry in freshwater flux which was also sufficient to eliminate the NPP solution.

Meridional overturning streamfunctions of the TH, SPP and NPP solutions for the case that the northern boundary is shifted 2 grid points towards the south ($\theta_N - 2$, implying that the boundary of the shelf lies at 52.5° N) are plotted in Fig. 3b-d. In absence of freshwater forcing ($F_0 = 0$), the southern cell of the TH state (Fig. 3b) is much stronger than the northern cell, because it is forced by lower atmospheric temperatures at high latitudes. For the reference value of $F_0 = 0.2$, both the SPP (Fig. 3c) and NPP (Fig. 3d)

states exist, but the MOC of the SPP state is slightly stronger.

The results in this and the previous subsection show that when multiple equilibria exist in an equatorially symmetric situation, any asymmetric effect (in forcing and geometry) can give rise to preference of specific solutions. It requires about a 22° asymmetry in basin extent to eliminate one of the pole-to-pole solutions. A similar elimination is induced by about a 0.76 mm day^{-1} difference between the freshwater forcing at 60° N and 60°S.

3 Preference in a global ocean model

With the notion of preference as explained in the previous section, we now turn to the steady state solutions of a global ocean-only model having a realistic continental geometry and bathymetry. As mentioned above four solutions were found for idealized two-basin configurations [Marotzke and Willebrand, 1991]. In Huisman et al. [2009], these solutions were labelled as C: Conveyor; IC: Inverse Conveyor; NS: Northern Sinking and SS: Southern Sinking. The issue addressed below is what remains of these solutions in a realistic global ocean geometry and a global asymmetric freshwater flux field.

3.1 Model formulation and freshwater forcing

A fully-implicit steady state ocean model is used in which the three-dimensional flow is governed by the hydrostatic, primitive equations in spherical coordinates, on a global domain which includes full continental geometry as well as bottom topography [Weijer et al., 2003; Dijkstra and Weijer, 2005; Huisman et al., 2010]. The horizontal resolution of the model is about 4° (a 96×38 Arakawa C-grid on a domain $[180°W, 180°E] \times [85.5°S, 85.5°N]$) and the grid has 12 non-equidistant levels in the vertical. The ocean flow is forced by

the annual-mean wind stress as given in Trenberth et al. [1989]. The upper ocean is coupled to a simple energy-balance atmospheric model [Dijkstra and Weijer, 2005] in which only the heat transport is modeled (no moisture transport); there is no sea-ice component. The thermal forcing consists of an annual mean prescribed equatorially symmetric short wave heat flux. Details of the model formulation and its strengths and weaknesses (e.g., relatively high friction and diffusion coefficients) are discussed in Dijkstra and Weijer [2005].

The special feature of this fully-implicit model is, similar to the 2D model above, that it has the ability to solve the steady model equations directly without using any time-marching techniques, and determines the 'true' steady states (with zero model drift) of the system. An additional advantage of the steady state model is that full bifurcation diagrams can be calculated and that the steady solutions determined satisfy integrated (freshwater) balances with a relative error smaller than 0.1%. Here, we use the same parameters setting and reference state as in Huisman et al. [2010].

When the model is forced by the satellite-based HOAPS [Andersson et al., 2010] freshwater flux (Fig. 4a) it is incapable of maintaining a Conveyor state; instead a Southern Sinking solution is found. The Conveyor state, with a strength of $15\,Sv$, can be retrieved when $0.14\,Sv$ of freshwater is subtracted from the North Atlantic. However, the surface salinity field found in this Conveyor state (Fig. 4b) does not resemble the observed SSS due to deficiencies in the ocean model. Therefore, as in Hughes and Weaver [1994], we choose to start with a restoring boundary condition for the salinity and diagnose the freshwater flux needed to maintain this salinity field.

The reference solution (referred to as case L) is calculated by restoring the model to the Levitus SSS field S_L (Fig. 5a, [Levitus et al., 1994]) with

a restoring time scale of 75 days. In this case, we find a Conveyor solution and diagnose the freshwater flux F_L from this steady state (Fig. 5c). The mean $E - P$ per unit area for the Atlantic Ocean (north of the equator and excluding the Arctic Ocean north of 74°N) is 0.15 mm day^{-1} (net evaporation) and for the Pacific Ocean (also north of the equator) it is -0.26 mm day^{-1} (net precipitation). The flux F_L hence is strongly asymmetric with net evaporation in the North Atlantic and net precipitation in the North Pacific as is (qualitatively) consistent with present-day observations [Zaucker et al., 1994; Talley, 2008; Andersson et al., 2010].

To create a freshwater flux with just the opposite east-west asymmetry, a second case (referred to as InvL) is defined by restoring to the SSS field S_{InvL} (Fig 5b), which is obtained by interchanging the Atlantic and Pacific SSS fields S_L. North of 60°N, zonally averaged values of the Levitus salinity field were used as only a few data points are available. A new steady state solution was computed from that of case L by defining the restoring salinity field $S = (1 - \alpha)S_L + \alpha\, S_{InvL}$, again with a restoring time of 75 days, and using a continuation in the parameter α from zero to one. Also for case InvL, the freshwater flux F_{InvL} is diagnosed (Fig. 5d). For this case, the mean $E - P$ per unit area is -0.17 mm day^{-1} for the Atlantic and 0.1 mm day^{-1} for the Pacific. Hence F_{InvL} and F_L have just an opposite east-west asymmetry.

To choose a control parameter, we follow the commonly used method to collapse the Atlantic MOC, usually referred to as 'hosing' [Rahmstorf et al., 2005]. An additional freshwater flux F_S^p is added over the area $(\phi, \theta) \in [60°W, 24°W] \times [54°N, 66°N]$ (cf. Fig. 6b, inset) and is zero elsewhere. The control parameter γ_{Atl} is the amplitude (in Sv) of this freshwater flux F_S^p and

hence for each case, the total freshwater flux is given by

$$F_S = F_S^d + \gamma_{Atl}\, F_S^p + Q, \tag{7}$$

where F_S^d is either F_L or F_{InvL} and Q is a compensating term to ensure a net zero freshwater flux over the total ocean surface.

3.2 Results

For both cases (L and InvL) the bifurcation diagrams (Fig. 6) show the maximum Atlantic (Fig. 6a) and Pacific (Fig. 6b) meridional overturning streamfunction versus the value of γ_{Atl} (in Sv). The upper branch of the bifurcation diagram for case L represents solutions with an Atlantic MOC having NADW formation. Under only the diagnosed freshwater flux field ($\gamma_{Atl} = 0$), we find a Conveyor state (label C, Atlantic and Pacific MOC patterns in Fig. 7a) where the maximum of the Atlantic streamfunction (Ψ_{Atl}) is $14\,Sv$. The deep Pacific cell is on the strong side due to the large diffusivities in the model. Considerable effort was spent trying to find other isolated solutions, without succeeding, so it appears that the Conveyor state is the unique state of case L at $\gamma_{Atl} = 0$.

At $\gamma_{Atl} = 0.23\,Sv$ a saddle-node bifurcation is reached. In 'hosing' experiments this is the point where the Atlantic MOC collapses [Rahmstorf et al., 2005]. The lower branch of solutions corresponds to stable steady states without NADW formation and the second saddle-node bifurcation (at $\gamma_{Atl} = 0.12\,Sv$) is related to the Atlantic MOC recovery in the 'hosing' experiments. Between the two saddle node bifurcation points a multiple equilibrium regime exists, where two different steady states are present under the same forcing conditions. The Pacific MOC is hardly affected by the change in γ_{Atl} and its pattern remains very similar to that in Fig. 7a. For large

values of γ_{Atl}, a SS state is found.

For the HOAPS freshwater flux, the bifurcation diagram was also calculated in case L (not shown), having a very similar shape as the drawn curve in Fig. 6a. However, the two saddle-node bifurcation points are shifted to negative values of γ_{Atl} with that on the lower branch located at $\gamma_{Atl} = -0.14\,Sv$. For the reference state ($\gamma_{Atl} = 0$) we hence find a Southern Sinking state. This reflects the deficiencies in the model to generate a global ocean circulation with a surface salinity field close to the Levitus one. However, when the freshwater flux is slightly adapted, for example by extracting 0.14 Sv from the Atlantic (see discussion Fig. 4 above), we effectively are using a value $\gamma_{Atl} = -0.14\,Sv$ and hence a Conveyor state can again be found. In a way, one can correct for the model deficiencies by modifying the freshwater flux, which is exactly the reason for using the diagnosed flux F_S^d in Fig. 6.

For case InvL, the bifurcation diagram is shown as the grey curves in Fig. 6. The different freshwater flux has clearly decreased the existence interval (in γ_{Atl}) of the C solution as the saddle node bifurcation on the upper branch has shifted to smaller values of γ_{Atl}. The C solution is now connected to the IC solution and a small isolated branch of the SS solution remains. Hence, under mixed boundary conditions there are at least two stable steady states for $\gamma_{Atl} = 0$. The first state (indicated by IC in Fig. 6) has no formation of NADW and has sinking in the North Pacific (Fig. 7b); this is the expected Inverse Conveyor state under the freshwater flux forcing of case InvL. The surprising result, however, is that there also exists a state with vigorous Atlantic overturning (indicated by label C in Fig. 6 and shown in Fig. 7c). The C and IC states of case InvL are connected by a branch of unstable steady states. As can be seen, besides these solutions, there exists an isolated branch for case InvL, illustrating that even under

the realistic global geometry, there is a small parameter range where more than two stable steady states exist (remaining from the original four states in the totally symmetric setup [Marotzke and Willebrand, 1991]). As these solutions only exist for a small interval of γ_{Atl} they are not further discussed here.

Note that $\gamma_{Atl} = 0$ is only an arbitrary reference value related to the equilibrium state which is determined under Levitus surface salinity conditions (from which the reference freshwater flux F_S^d is diagnosed). In the results above, it is hence important that there exists an interval of overlap of the conveyor solutions for both cases L and InvL and not that this interval should enclose $\gamma_{Atl} = 0$.

The different SSS fields for the circulation patterns of Fig. 7 are shown in Fig. 8. Due to the presence of NADW formation in the Atlantic, the SSS of the C solution in case InvL (Fig. 8c) is up to 2 g/kg larger than the surface salinity of solution IC (Fig. 8b), with maximum salinification in the northern North Atlantic. This gives rise to a SSS pattern in the Atlantic, caused by the circulation, that resembles the Levitus salinity field (Fig. 8a) even with a large net precipitation over the Atlantic.

The global SST difference between the C solutions (at $\gamma_{Atl} = 0$) in case L and that in case InvL (Fig. 9a) shows that the North Atlantic is only slightly warmer in case L, while the North Pacific is up to 1.5 °C cooler. The North Pacific is saltier in case InvL than in case L (Fig. 9b), apart from a region near the Asian continent. The North Atlantic is fresher in case InvL than in case L as can also be seen from Fig. 8. The SSS contrast between Atlantic and Pacific is smaller for the InvL (C) case than for the L (C) case, consistent with the weaker North Atlantic MOC, but there still is a SSS contrast with the northern North Atlantic being saltier than the northern North Pacific.

The interesting result is that apparently the Atlantic MOC (through the salt-advection feedback) can more efficiently transport salty subtropical waters northward than the Pacific MOC to allow for a C solution to exist in the case InvL.

4 Summary, Discussion and Conclusions

In this paper we have determined steady state solutions of a global ocean model for two very different surface freshwater flux patterns to investigate the effect of strong Pacific-Atlantic freshwater forcing asymmetries on the global ocean circulation. Complementary to the results in Hughes and Weaver [1994], de Boer et al. [2008] and Ferreira and Marshall [2010], we systematically explored the steady solutions in parameter space and presented full bifurcation diagrams instead of performing a limited set of time integrations. In addition, the present-day ocean geometry and bathymetry are better represented.

It needs to be stressed that the model used is very low-resolution and highly diffusive and has only a linear equation of state. In addition, the atmospheric model to which it is coupled is only an energy balance model, so it is not suited for quantitative studies of the global ocean circulation. However, we can study the effect of freshwater flux asymmetries on the global ocean circulation due to only the salt-advection feedback, as this mechanism is represented adequately in this model.

Although different equilibria of the MOC have been recently found in the FAMOUS model [Hawkins et al., 2011], it has been difficult in GCMs (as used in IPCC - AR4) to find off-states (Southern Sinking states) of the MOC. There are, however, two arguments based on recent results which indicate

that the Atlantic MOC may be much more sensitive to freshwater anomalies than these GCMs indicate. The first issue concerns the bias in the Atlantic freshwater budget of the GCMs as shown in Drijfhout et al. [2010]. Because of this bias, the equilibrium MOC states export salt out of the Atlantic basin and hence no transition to a collapsed state can occur [Huisman et al., 2010]. From observations (and also reanalysis results), the present-day MOC appears to export freshwater out of the Atlantic basin and hence an off-state may exist [Hawkins et al., 2011]. The second argument is that the strength of the ocean-atmosphere feedbacks is by far too weak to remove the multiple equilibrium regime as was recently shown in Den Toom et al. [2012].

Our main aim was to investigate the preference of the Conveyor (C) and Inverse Conveyor (IC) states under the different freshwater fluxes applied, where the concept of preference was defined using a two-dimensional model. The bifurcation diagrams in Fig. 6 shows that continental asymmetry is very effective in selecting equilibria as not many of the original 4 equilibria in the idealized two-basin case [Huisman et al., 2009] remain. Under the freshwater flux which is needed to maintain the Levitus SSS field, only the C state is found and the IC state is absent. The model has a multiple equilibrium regime, because in addition to the Conveyor, also the Southern Sinking (SS) solution is found for larger values of γ_{Atl}.

If the freshwater forcing were the dominant asymmetry in setting the pattern of the Conveyor (C) solution, one would expect to find only the Inverse Conveyor (IC) state under the freshwater flux which is needed to maintain the inverse Levitus SSS (case InvL). However, we find two stable equilibria in this case: the IC state state (with North Pacific sinking) and a weaker (than in the Levitus case) C state (with North Atlantic sinking). This means that, with a freshwater flux giving net precipitation (evaporation) over

the Atlantic (Pacific) there still exists a C state. The existence of a weak C state is remarkable as it shows that the continental geometry possibly plays a substantial role in the preference of the different MOC solutions with respect to changes in freshwater flux. The physics is, as suggested by de Boer et al. [2008], that the Atlantic is more efficient to transport subtropical salty water northwards than the Pacific and hence provides a stronger response to asymmetries through the salt-advection feedback.

From the results of this global ocean model, admittedly with all its limitations, we therefore find that other factors than the freshwater flux asymmetry likely play a role to produce the Atlantic-Pacific asymmetric overturning. The asymmetry in the surface freshwater flux pattern will certainly affect the global ocean circulation but it cannot be dominantly responsible for the preference of the North Atlantic deep water formation. Our results point to the impact of continental asymmetries inducing a preference for Atlantic sinking. However, because we did not determine the possible global equilibria under deformation of the present-day ocean geometry we are not able to indicate which aspects of the geometry are most affecting this selection of equilibria; this is left for further study.

Acknowledgments

The computations were done on the Huygens IBM Power6 at SARA in Amsterdam and on the facilities available to Los Alamos National Laboratories. Use of the SARA computing facilities was sponsored by the National Computing Facilities Foundation (N.C.F.) under the project SH084-08 with financial support from the Netherlands Organization for Scientific Research (NWO). The authors thank Matthijs den Toom (IMAU) for his help in generating the results in section 2 of this paper and the referees and editor for the very useful comments on the first version of this paper.

References

Andersson, A., K. Fennig, C. Klepp, S. Bakan, H. Graßl, and J. Schulz, 2010: The Hamburg Ocean Atmosphere Parameters and Fluxes from Satellite Data – HOAPS-3. *Earth System Science Data*, **2**, 215–234.

Czaja, A., 2009: Atmospheric Control on the Thermohaline Circulation. *Journal Of Physical Oceanography*, **39**, 234–247.

De Boer, A. M., J. R. Toggweiler, and D. M. Sigman, 2008: Atlantic Dominance of the Meridional Overturning Circulation. *Journal Of Physical Oceanography*, **38**, 435–450.

Den Toom, M., H. Dijkstra, A. Cimatoribus, and S. Drijfhout, 2012: Effect of Atmospheric Feedbacks on the Stability of the Atlantic Meridional Overturning Circulation. *J. Climate, in press, doi: 10.1175/JCLI-D-11-00467.1.*

Dijkstra, H. A., 2005: *Nonlinear Physical Oceanography.* Springer, 2nd edition.

Dijkstra, H. A. and M. J. Molemaker, 1997: Symmetry breaking and overturning oscillations in thermohaline-driven flows. *Journal of Fluid Mechanics*, **331**, 169–198.

Dijkstra, H. A. and W. Weijer, 2005: Stability of the Global Ocean Circulation: Basic Bifurcation Diagrams. *Journal Of Physical Oceanography*, **35**, 933–948.

Drijfhout, S., S. Weber, and E. van der Swaluw, 2010: The stability of the MOC as diagnosed from model projections for pre-industrial, present and future climates. *Climate Dynamics*, **40**, 1–12.

518 Emile-Geay, J., M. A. Cane, N. Naik, R. Seager, A. C. Clement, and A. van
519 Geen, 2003: Warren revisited: Atmospheric freshwater fluxes and "Why
520 is no deep water formed in the North Pacific". *Journal Of Geophysical*
521 *Research-Oceans*, **108**, 3178–3188.

522 Ferreira, D. and J. Marshall, 2010: Localization of deep water formation:
523 Role of atmospheric moisture transport and geometrical constraints on
524 ocean circulation. *Journal Of Climate*, **23**, 1456–1466.

525 Ferrari, F. and Ferreira, D., 2011: What processes drive the ocean heat
526 transport?. *Ocean Modelling*, **38**, 171–186.

527 Ganachaud, A. and C. Wunsch, 2000: Improved estimates of global ocean
528 circulation, heat transport and mixing from hydrographic data. *Nature*,
529 **408**, 453–457. 10.1038/35044048.

530 Hawkins, E., R. S. Smith, L. C. Allison, J. M. Gregory, T. J. Woollings,
531 H. Pohlmann, and B. De Cuevas, 2011: Bistability of the Atlantic over-
532 turning circulation in a global climate model and links to ocean freshwater
533 transport. *Geophysical Research Letters*, **38**(10), L10605.

534 Hughes, T. M. C. and A. J. Weaver, 1994: Multiple Equilibria of an Asym-
535 metric Two-Basin Ocean Model. *Journal Of Physical Oceanography*, **24**,
536 619–637.

537 Huisman, S. E., M. den Toom, H. A. Dijkstra, and S. Drijfhout, 2010: An
538 Indicator of the Multiple Equilibria Regime of the Atlantic Meridional
539 Overturning Circulation. *Journal Of Physical Oceanography*, **40**, 551–567.

540 Huisman, S. E., H. A. Dijkstra, A. von der Heydt, and W. P. M. De Ruijter,

2009: Robustness of multiple equilibria in the global ocean circulation. *Geophysical Research Letters*, **36**, L01610.

Levitus, S., R. Burgett, and T. P. Boyer, 1994: *World Ocean Atlas 1994, Volume 3: Salinity*. NOAA Atlas NESDIS 3, US Department of Commerce, Washington, D.C.

Marotzke, J. and J. Willebrand, 1991: Multiple Equilibria of the Global Thermohaline Circulation. *Journal Of Physical Oceanography*, **21**, 1372–1385.

Rahmstorf, S., M. Crucifix, A. Ganopolski, H. Goosse, I. Kamenkovich, R. Knutti, G. Lohmann, R. Marsh, L. A. Mysak, Z. Wang, and A. J. Weaver, 2005: Thermohaline circulation hysteresis: A model intercomparison. *Geophysical Research Letters*, **32**, L23605.

Talley, L. D., 2003: Shallow, Intermediate, and Deep Overturning Components of the Global Heat Budget *Journal Of Physical Oceanography*, **33**, 530–560.

Talley, L. D., 2008: Freshwater transport estimates and the global overturning circulation: Shallow, deep and throughflow components *Progress in Oceanography*, **78**, 257–303.

Trenberth, K. E., J. G. Olson, and W. G. Large, 1989: A global ocean wind stress climatology based on ECMWF analyses. Technical report, Boulder, CO, U.S.A.

von der Heydt, A. and H. A. Dijkstra, 2008: The effect of gateways on ocean circulation patterns in the Cenozoic. *Global And Planetary Change*, **62**(1-2), 132–146.

565 Warren, B. A., 1983: Why is no deep water formed in the North Pacific.
566 *Journal Of Marine Research*, **41**, 327–347.

567 Weaver, A. J., C. M. Bitz, A. F. Fanning, and M. M. Holland, 1999: Ther-
568 mohaline circulation: High-latitude phenomena and the difference between
569 the Pacific and Atlantic. *Annual Review of Earth and Planetary Sciences*,
570 **27**, 231–285.

571 Weijer, W. and H. A. Dijkstra, 2001: A bifurcation study of the three-
572 dimensional thermohaline ocean circulation: The double hemispheric case.
573 *Journal Of Marine Research*, **33**, 599–631.

574 Weijer, W., H. A. Dijkstra, H.Oksuzoglu, F. W. Wubs, and A. C. de Niet,
575 2003: A fully-implicit model of the global ocean circulation. Weijer,
576 Wilbert, Henk A Dijkstra, Hakan Oksuzoglu, Fred W. Wubs, and Arie
577 C. de Niet. 2003. Journal of Computational Physics 192 (2) (December):
578 452 – 470.

579 Zaucker, F., T. F. Stocker, and W. S. Broecker, 1994: Atmospheric freshwater
580 fluxes and their effect on the global thermohaline circulation. *Journal of*
581 *Geophysical Research*, **99**, 12,443-12,457.

List of Figures

Parameter	Meaning	Value	Dimension
r_0	radius of the earth	$6.4 \cdot 10^6$	m
ρ_0	reference density	$1.0 \cdot 10^3$	kg m^{-3}
D	open ocean depth	4000	m
g	gravitational acceleration	9.8	ms^{-2}
A_V	vertical viscosity	$1.0 \cdot 10^{-3}$	m^2 s^{-1}
A_H	horizontal viscosity	$2.2 \cdot 10^{12}$	m^2 s^{-1}
K_V	vertical diffusivity	$1.0 \cdot 10^{-4}$	m^2 s^{-1}
K_H	horizontal diffusivity	$1.0 \cdot 10^3$	m^2 s^{-1}
α_T	compressibility of heat	10^{-4}	K^{-1}
α_S	compressibility of salt	$7.6 \cdot 10^{-4}$	-
S_0	reference salinity	35	g kg^{-1}
T_0	reference temperature	15	K

Table 1: Standard values of parameters used in the numerical calculations.

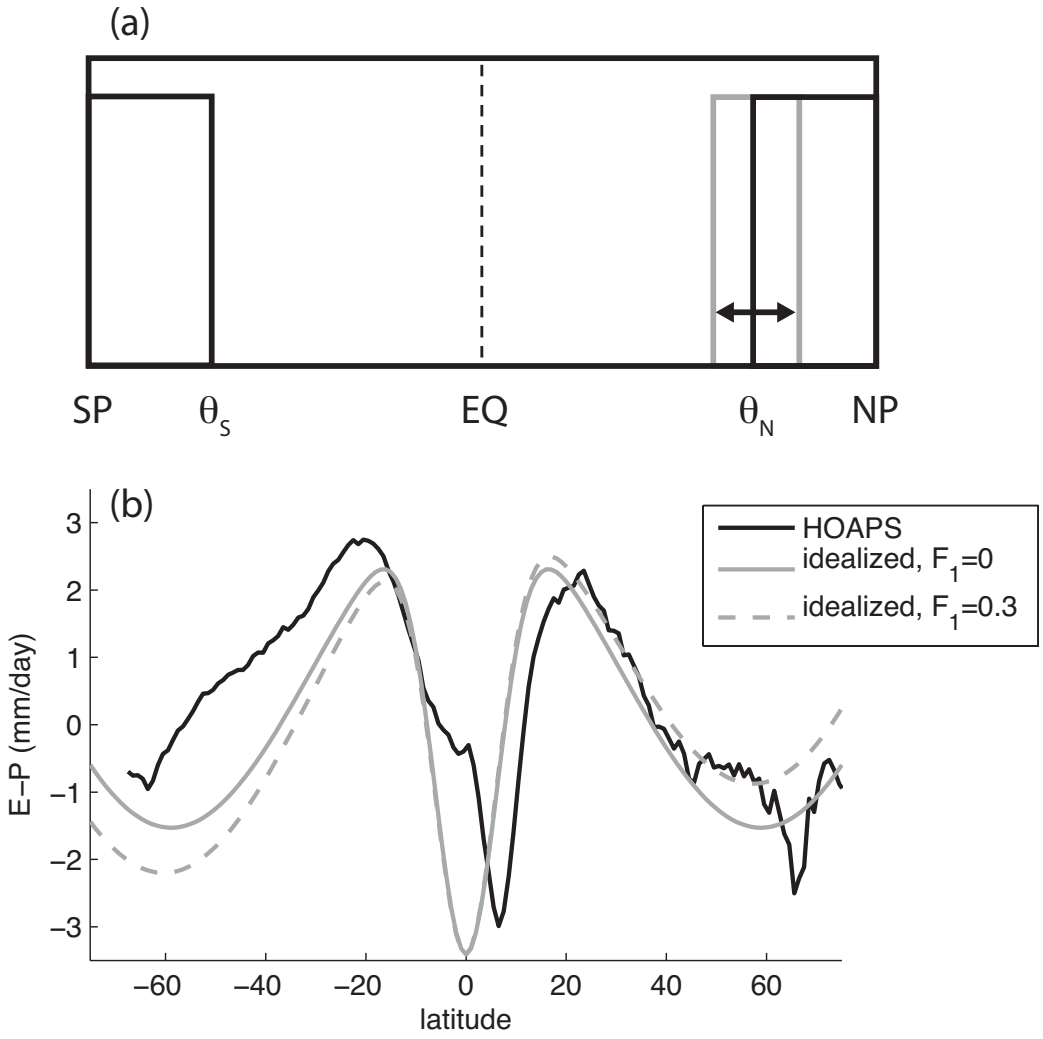

Figure 1: (a) Basin setup with a model domain bounded by latitudes between $75°S$ and $75°N$. The shallow regions are only 500 m deep with fixed latitude $\theta_S = 60°S$ and where θ_N is variable. (b) Freshwater flux (F_S, E-P) from data (zonally averaged from the HOAPS dataset [Andersson et al., 2010] and idealized profiles for $\mathcal{A} = 10$ mm day^{-1}, $F_0 = 0.225$ and $F_1 = 0$ (drawn grey) and $F_1 = 0.3$ (dashed grey). The profiles have a zero surface integral. Values in mm day^{-1}.

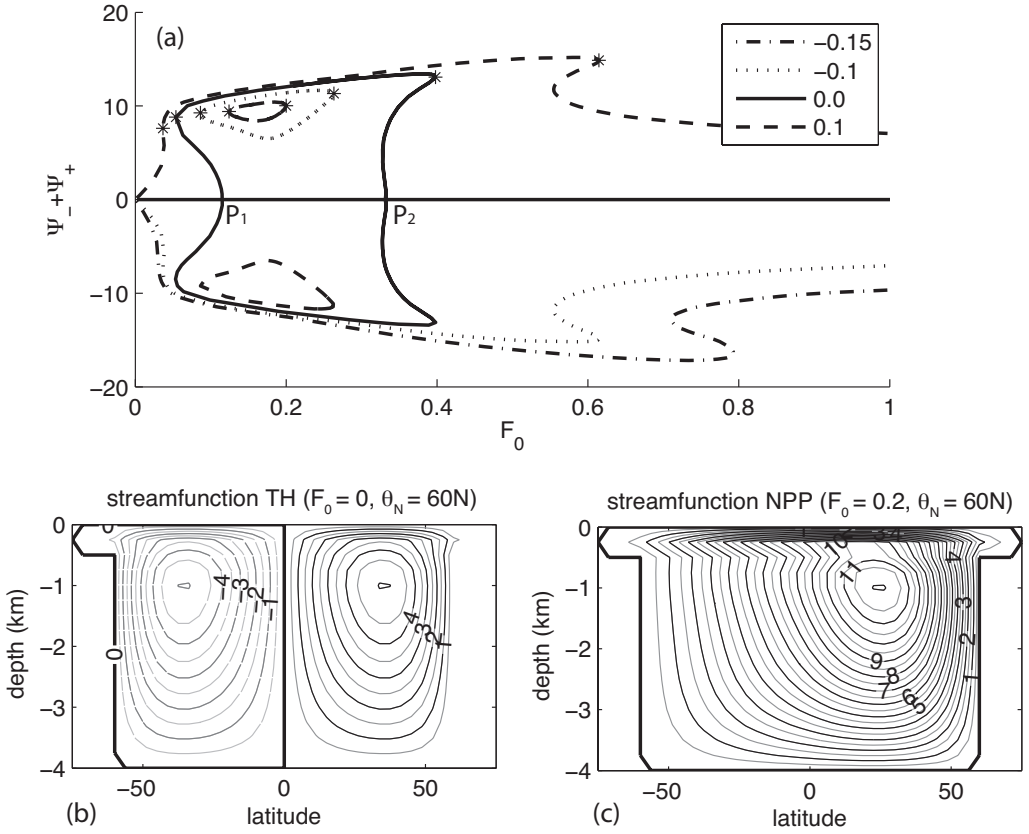

Figure 2: *(a)* $\Psi_- + \Psi_+$ *(Sv) against the amplitude parameter* F_0 *in the freshwater flux for symmetric hemispheres. Line styles indicate different values of the asymmetry parameter* F_1 *and the stability of the solutions is not indicated.* P_1 *and* P_2 *are the pitchfork bifurcation points associated with the symmetry breaking in the TH and SA solutions. Stars mark the existence interval of the stable NPP solution (*$I_{F_1}[NPP]$*). (b-c) Meridional overturning streamfunction (Sv) for solutions at the drawn branch in (a) for the symmetric freshwater forcing (*$F_1 = 0$*). (b) TH state (*$F_0 = 0$*) and (c) NPP state (*$F_0 = 0.2$*). Values in Sverdrup.*

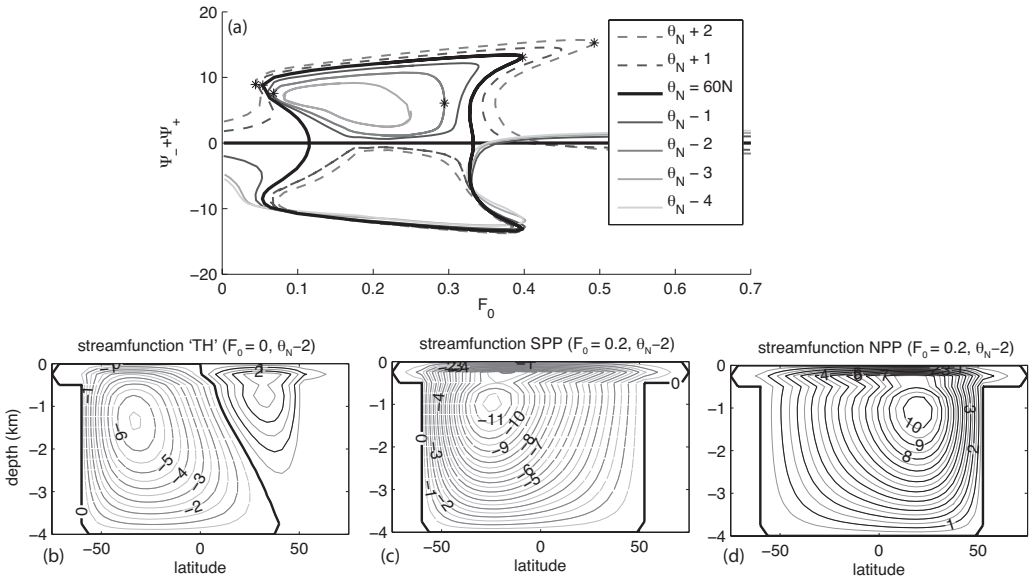

Figure 3: *(a)* $\Psi_- + \Psi_+$ *(Sv) versus the freshwater forcing amplitude* F_0 *for different values of* θ_N*, where* $+1$ (-1) *means one grid-point* (3.75°) *more northwards (southwards). Stars mark the existence interval of the NPP solution (*$I_{\theta_N}[NPP]$*). The asymmetry parameter* $F_1 = 0$*. (b-d) Meridional overturning streamfunctions (Sv), with asymmetric hemispheres (*$\theta_N - 2$*, where* -2 *again denotes 2 gridpoints, i.e.* 7°*, equatorward) and symmetric freshwater forcing* $(F_1 = 0)$*. (b) TH state (*$F_0 = 0$*); (c) SPP state (*$F_0 = 0.2$*); (d) NPP state (*$F_0 = 0.2$*). Note that the SPP and NPP states are not of the same strength, because the extent of the northern hemisphere is smaller than the southern hemisphere.*

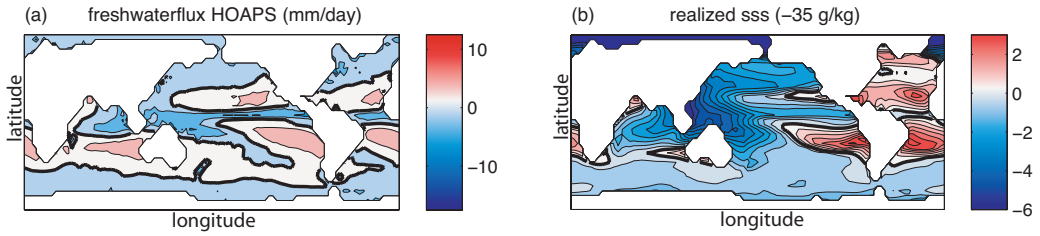

Figure 4: *(a) Surface freshwater flux ($mm\,day^{-1}$) adapted for the model grid from the HOAPS data set [Andersson et al., 2010]; (b) surface salinity fields ($-35\,g\,kg^{-1}$) realized for the Conveyor solution under the flux from (a). This Conveyor solution is found when $0.14\,Sv$ of freshwater is subtracted from the North Atlantic.*

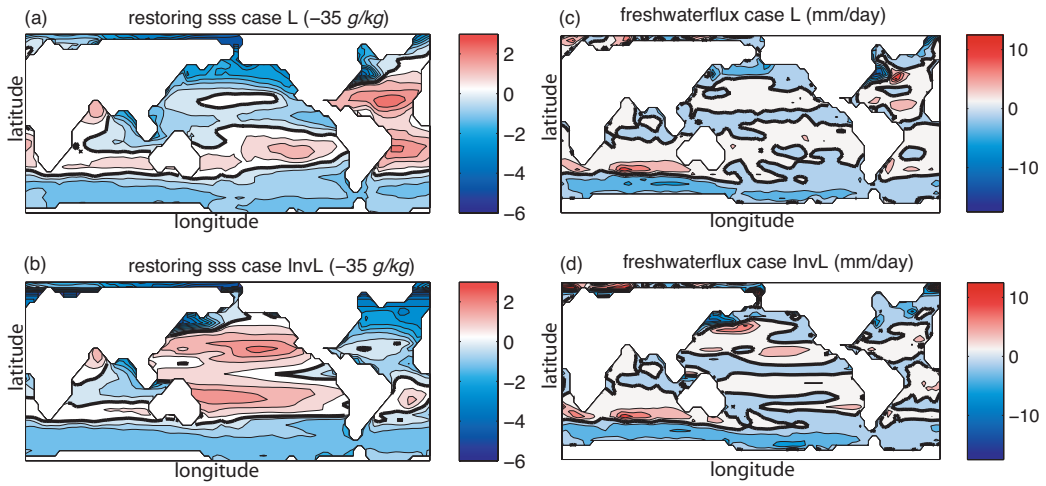

Figure 5: *(a-b) Surface salinity fields* ($-35\,g\,kg^{-1}$) *used for restoring forcing and diagnosed freshwater fluxes* ($mm\,day^{-1}$) *in the two experiments. (a) Levitus salinity field* S_L *[Levitus et al., 1994]; (b) Inverse Levitus salinity field* S_{InvL}*; this field is obtained by interchanging the Atlantic and Pacific SSS of the field under (a).* S_{InvL} *is corrected with a constant factor (of* $0.2\,g/kg$*), surface integral of salinity remains unchanged. (c) diagnosed freshwater flux* F_L *for cases* L *and (d)* F_{InvL} *for case* $InvL$*. The large scale patterns are represented: net precipitation around the equator and at high latitudes, and net evaporation in the subtropics.*

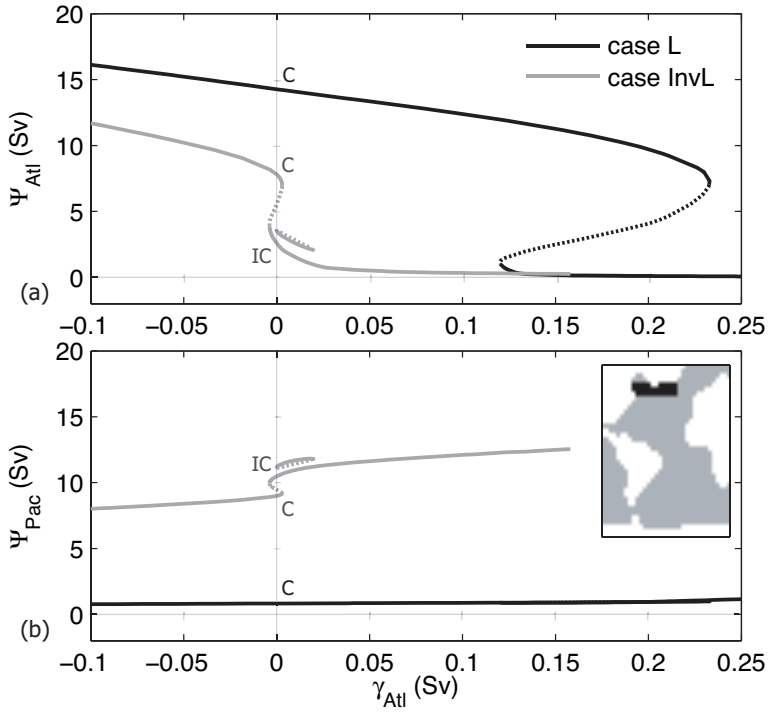

Figure 6: *Bifurcation diagram under mixed boundary conditions in which the maximum value of the meridional overturning streamfunction in (a) the Atlantic (Ψ_{Atl}) and (b) the Pacific (Ψ_{Pac}) are plotted versus the amplitude of the freshwater forcing in the North Atlantic (γ_{Atl}, the area over which the flux is changed is shown in the inset). Both streamfunction values are the maximum values below 500 m. Drawn (dotted) branches represent stable (unstable) steady states. The labels refer a Conveyor type solution (C) and an Inverse Conveyor type solution (IC), of which the streamfunctions are plotted in Fig. 7. In (a) the isolated branch for case InvL is shifted upwards with* $1\,Sv$*, to make it visible.*

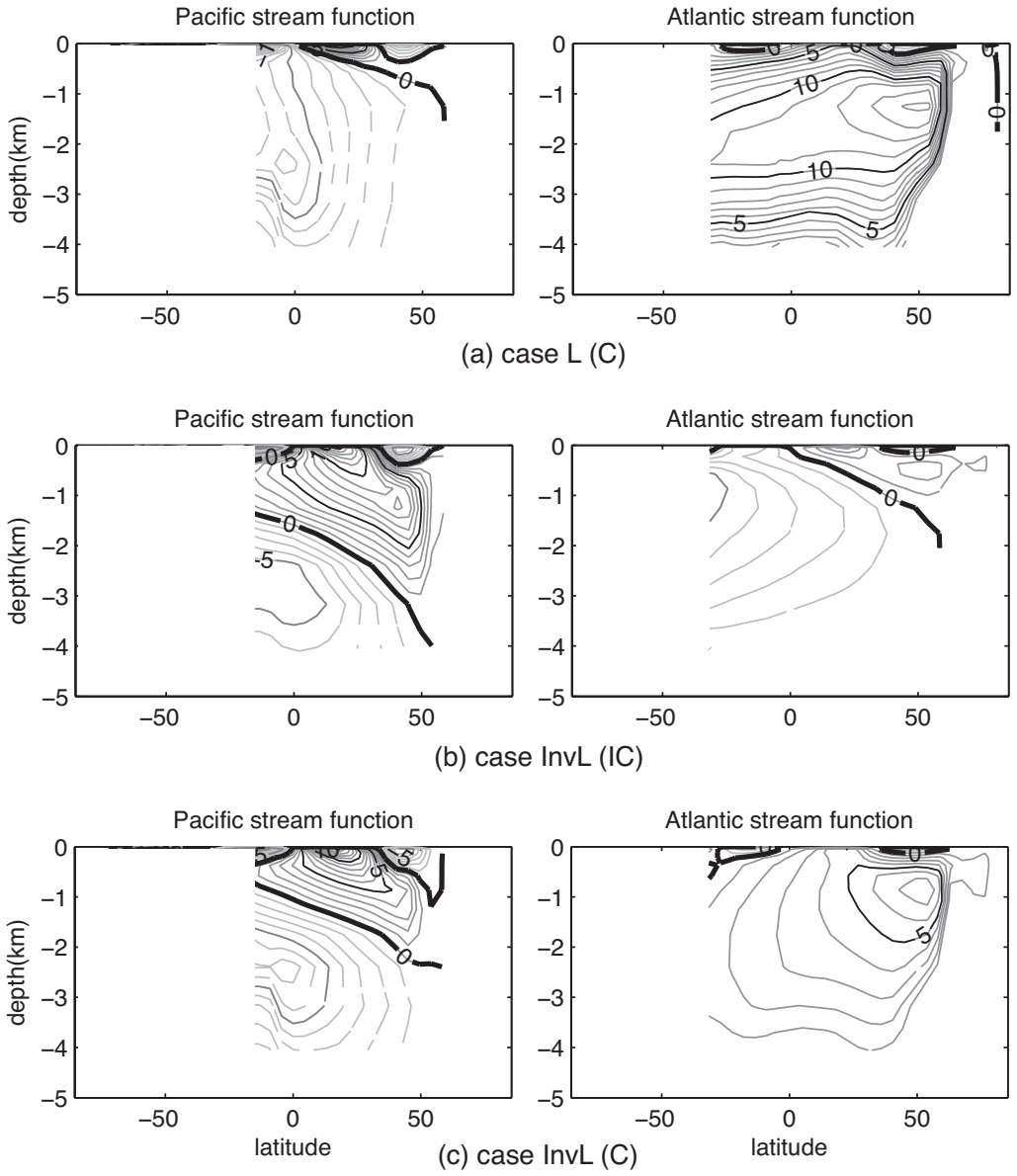

Figure 7: *Meridional overturning streamfunction in Pacific (left) and Atlantic (right), under mixed boundary conditions for* $\gamma_{Atl} = 0$ *in Fig. 6. (a) Conveyor type solution (C) for case L with deep water formation confined to the North Atlantic; (b) Inverse Conveyor type solution (IC) for case InvL with deep water formation in the North Pacific. (c) Conveyor type solution (C) for case InvL with deep water formation in the North Atlantic.*

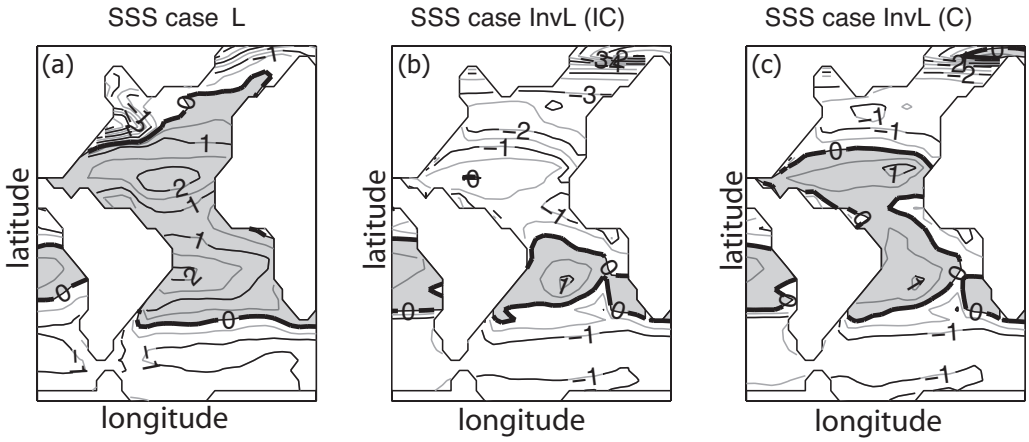

Figure 8: *SSS realized under mixed boundary conditions (for solutions with* $\gamma_{Atl} = 0$*). The presence of the overturning cell in the Conveyor type solution (C) for case InvL (c) provides a salinification of the Atlantic up to* $2\,psu$ *with respect to the Inverse Conveyor type solution (IC) without NADW formation (b). For reference also the SSS for the Conveyor type solution (C) in case L is shown (a).*

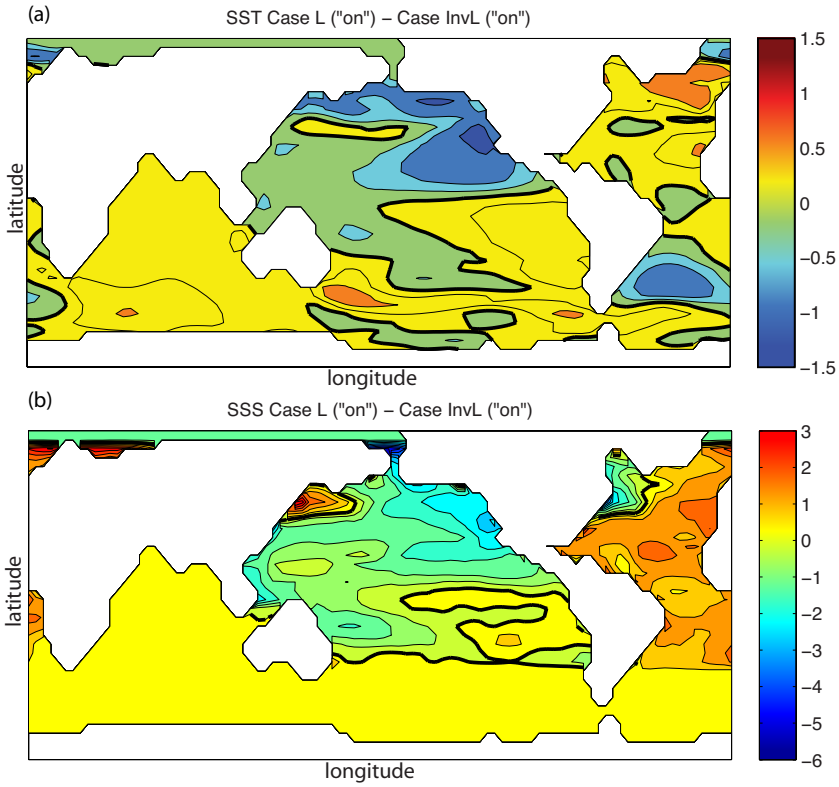

Figure 9: *(a) SST (°C) and (b) SSS (psu) difference between the Conveyor type solutions (C) for the cases L and InvL (at* $\gamma_{Atl} = 0$*).*